Acta Mechanica Solida Sinica
https://doi.org/10.1007/s10338-024-00532-1

FULL-LENGTH ARTICLE

Indentation of a Plate on a Thin Transversely Isotropic Elastic Layer

Juyao Li[1] · Guozheng Zhang[1] · Liu Wang[2,3] · Zhaohe Dai[1]

Received: 29 May 2024 / Revised: 26 August 2024 / Accepted: 3 September 2024

Abstract
This work investigates the indentation response of an elastic plate resting upon a thin, transversely isotropic elastic layer supported by a rigid substrate. Such a scenario is encountered across a range of length scales from piezoresistive tests on graphite nanoflakes to the bending of floating ice shelves atop seabed, where the elastic layer commonly exhibits certain anisotropy. We first develop an approximate model to describe the elastic response of a transversely isotropic layer by exploiting the slenderness of the layer. We show that this approximate model can be reduced to the classic compressible Winkler foundation model as the elastic constants of the layer are set isotropic. We then investigate the combined response of an elastic plate on the transversely isotropic elastic layer. Facilitated by the simplicity of our proposed approximate model, we can derive simple analytical solutions for the cases of small and large indenter radii. The analytical results agree well with numerical calculations obtained via finite element methods, as long as the system is sufficiently slender in a mechanical sense. These results offer quantitative insights into the mechanical behavior of numerous semiconductor materials characterized by transverse isotropy and employed with slender geometries in various practical applications where the thin layer works as conductive and functional layers.

Keywords Indentation · Elastic layers · Transversely isotropic · Winkler foundation · Graphite

1 Introduction

In experimental mechanics at small scales, applying a point-like indentation force and measuring the mechanical response of the material under such a load is one of the most effective methods to reveal the elastic properties of nanoscale materials, such as ultrathin membranes, nanoplates, nanoribbons, and nanowires [1–5].

The material response under indentation, however, largely depends on the way the material is supported. There are two typical scenarios in general [6, 7]. One well-explored scenario involves the slender nanomaterial being suspended over a trench or a cavity with its edges somewhat clamped by the contacting substrate [2, 8]. In this case, the material responds to the applied indentation force by stretching and bending (essentially stretching and compression across a neutral axis) [9], which allows the measurement of in-plane elastic properties [10–13]. For measuring the out-of-plane properties of nanomaterials, such as the *c*-axis modulus of a graphite nanoflake [6, 14], the second scenario is used, where the slender nanomaterial is fully supported by a relatively rigid substrate. In particular, another highly conductive plate is often coated on such supported nanomaterials in piezoresistive tests or electronic device applications to ensure good conductivity across the interface (see Fig. 1a) [6, 15, 16]. This work focuses on the second scenario, specifically the indentation response of an elastic plate coating on a nanomaterial supported by a rigid substrate (Fig. 1b). In this case, the sandwiched slender nanomaterial behaves as a thin, elastic layer. The problem we consider here, therefore, evokes the classic Winkler foundation problem, where a transverse force is applied to a plate resting on an elastic foundation [17]. The key to our problem lies in determining the effective foundation stiffness of the elastic layer.

✉ Zhaohe Dai
daizh@pku.edu.cn

1 State Key Laboratory for Turbulence and Complex Systems, Department of Mechanics and Engineering Science, College of Engineering, Peking University, Beijing 100871, China

2 CAS Key Laboratory of Mechanical Behaviour and Design of Materials, Department of Modern Mechanics, University of Science and Technology of China, Hefei 230026, Anhui, China

3 State Key Laboratory of Nonlinear Mechanics, Institute of Mechanics, Chinese Academy of Science, Beijing 100190, China

Published online: 07 October 2024

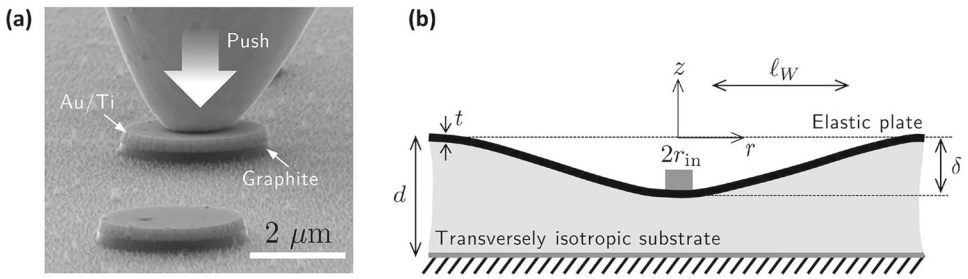

Fig. 1 Indentation of a plate on an elastic layer: **a** SEM image of a typical indentation experiment involving a metal plate on a graphite layer (courtesy of Xianlong Wei); **b** schematic and notations of the model, where the plate is assumed to be isotropic and the substrate is considered transversely isotropic

Extensive discussions have explored the mechanical behavior of linear isotropic elastic layers, from the classical Boussinesq model for a half-space [18] to Winkler's mattress model for very thin layers. In particular, thin layers have been studied in various contexts, including compressible [19], incompressible [20], and nearly incompressible [21–23]. Our investigation diverges from these studies by focusing on an anisotropic (specifically, transversely isotropic) elastic layer, such as graphite nanoflakes. The out-of-plane properties of a transversely isotropic elastic layer differ from its in-plane properties [24], necessitating the use of this type of indentation test to reveal all components of the elasticity tensor. Notably, configurations involving an elastic plate on a transversely isotropic elastic layer can be found not only in nanoscale electronic devices [6, 14] but also in a range of natural and engineering systems including a tensioned cell cortex on a foundation-like cytoplasm [25] and a bending ice sheet on the seabed [26].

Many efforts have been made to understand the mechanical response of transversely isotropic elastic layers. For example, Elliott studied indentation on transversely isotropic half-spaces using punches of arbitrary axisymmetric shape [27]. Fabrikant employed an integral transform method, expressing three potential functions as a sum of the potential functions for a half-space, and provided an elementary solution to contact problems for a transversely isotropic elastic layer [28]. Using Fabrikant's method, solutions for sliding contact problems in transversely isotropic half-spaces were obtained [29, 30]. Ding and Xu derived general solutions for axisymmetric problems in transversely isotropic spaces using stress functions [31]. Yu et al. introduced the point-force Green's function for a transversely isotropic elastic layer, which can be applied to solve indentation problems [32, 33]. Ning et al. developed approximate solutions for the mechanical response of a thin, transversely isotropic elastic layer on a rigid substrate using simplified kinematics [34]. More recently, Argatov and Mishuris derived asymptotic solutions for the contact problem of thin compressible and incompressible transversely isotropic elastic layers [35]. Despite such progress, the combined indentation response of plates on transversely isotropic elastic layers remains unexplored to the best of our knowledge.

In this study, we investigate the indentation response of an elastic plate bonded to a thin, transversely isotropic elastic layer supported by a rigid substrate using transform methods. Specifically, we provide the linear normal force–deformation relation for a transversely isotropic elastic layer of finite thickness in the Hankel space, which has not been reported previously. Though this approach would limit the problem to be axisymmetric, we are able to discuss the Hankel-space Green's function for half-spaces and compressible thin layers and then verify that these results can reduce to the classic Green's functions for isotropic half-spaces and isotropic elastic thin layers by setting the elastic constants to be isotropic. Using these tools, we derive the indentation force-depth relation for plates on transversely isotropic elastic layers in large and small indenter limits. The analytical solutions show good agreement with numerical calculations using finite element methods. We also discuss the limitations of our solution. These results offer quantitative insights into the mechanical behavior of various semiconductor materials characterized by transverse isotropy and used in slender geometries in practical applications.

2 The Model

2.1 Problem Description

In this section, we discuss governing equations for an elastic plate of thickness t and bending rigidity B on a thin, transversely isotropic elastic layer supported by a rigid substrate. Without loss, we assume axisymmetry and perfect bonding between the plate and elastic layer as well as between the elastic layer and the rigid substrate. In addition, we consider a constant, prescribed displacement δ within the region $r < r_{\text{in}}$ (see Fig. 1b), analogous to using a rigid cylindrical indenter of radius r_{in} to indent the elastic plate.

Upon indentation, a lateral characteristic length ℓ_W emerges, over which the indented displacement gradually smears out (Fig. 1b). Determining this length requires understanding the elastic response of both the plate and the substrate. In typical piezoresistive tests [6], the indentation depth δ is much smaller than the thickness of the plate t.

Thus, we employ the linear Kirchhoff–Love plate theory to characterize the mechanical response of the plate. We will show that both the in-plane shear traction between the plate and the substrate and the shear deformation of the plate can be neglected to the leading order (i.e., when $t, d \ll \ell_W$). The governing equation for the plate is then

$$B\nabla_{\mathrm{H}}^4\zeta(r) = q(r) + p(r) \tag{1}$$

where $z = \zeta(r)$ represents the deflected shape of the plate, $\nabla_{\mathrm{H}}^2 = \partial^2/r^2 + \partial/r\partial r$ is 2D axisymmetric Laplacian, p is the load applied by the indenter to ensure the prescribed displacement, and q is the reaction of the thin elastic layer (positively defined upward). To specify this reaction, we next examine the mechanical response of the transversely isotropic elastic layer.

2.2 Transversely Isotropic Elastic Substrate

We exploit the linear kinematic relations between six strain components (ε_r, ε_θ, ε_z, $\gamma_{r\theta}$, γ_{rz}, and $\gamma_{\theta z}$) and three components of the displacement vector: radial displacement u_r, hoop displacement u_θ, and transverse displacement u_z. The material properties are the same in all directions in the lateral plane in Fig. 1b and different from those along the z-axis. In this case, there are five independent constants in the (fourth-rank) elasticity tensor (reduced from a total of 21 independent constants in the case of full anisotropicity). Specifically, the Hooke's relation between strain and stress components reads

$$\begin{aligned}
\varepsilon_r &= a_{11}\sigma_r + a_{12}\sigma_\theta + a_{13}\sigma_z\\
\varepsilon_\theta &= a_{12}\sigma_r + a_{11}\sigma_\theta + a_{13}\sigma_z\\
\varepsilon_z &= a_{13}(\sigma_r + \sigma_\theta) + a_{33}\sigma_z\\
\gamma_{\theta z} &= a_{44}\tau_{\theta z}\\
\gamma_{rz} &= a_{44}\tau_{rz}\\
\gamma_{r\theta} &= 2(a_{11} - a_{12})\tau_{r\theta}
\end{aligned} \tag{2}$$

where $a_{11} = 1/E$, $a_{12} = -\nu/E$, $a_{33} = 1/E'$, $a_{13} = -\nu'/E'$, $a_{44} = 1/G'$; E and E' are Young's moduli in the symmetry plane and in the direction normal to it (i.e., the vertical plane), respectively; ν and ν' are Poisson's ratios characterizing the lateral strain response in the symmetry and vertical planes, respectively; and G' is the shear modulus in planes normal to the symmetry plane. It can be readily shown that, with axisymmetry, $u_\theta = 0$, and the components including $\gamma_{\theta z}$, $\gamma_{r\theta}$, $\tau_{\theta z}$, and $\tau_{r\theta}$ vanish. Now, similar to Sneddon's approach to axisymmetric, isotropic systems [36], we put the non-vanishing components of the displacement vector as [37]:

$$u_r = -\frac{(a_{11} - a_{12})(-2a_{13}^2 - a_{44}a_{13} + a_{11}a_{33} + a_{12}a_{33})}{a_{11}a_{33} - a_{13}^2}\frac{\partial^2\Phi}{\partial r\partial z} \tag{3}$$

and

$$u_z = \left[a_{44}\frac{\partial^2}{\partial r^2} + a_{44}\frac{\partial}{r\partial r} - \frac{(-a_{33}a_{11}^2 + 2a_{11}a_{13}^2 + a_{33}a_{12}^2 - 2a_{12}a_{13}^2)}{a_{11}a_{33} - a_{13}^2}\frac{\partial^2}{\partial z^2}\right]\Phi \tag{4}$$

where Φ is an arbitrary function. With these equations, we combine Hooke's relation in Eq. (2) and linear kinematics to obtain non-vanishing components of stress in Φ:

$$\begin{aligned}
\sigma_r &= -\frac{\partial}{\partial z}\left(\frac{\partial^2}{\partial r^2} + \frac{b}{r}\frac{\partial}{\partial r} + a\frac{\partial^2}{\partial z^2}\right)\Phi\\
\sigma_\theta &= -\frac{\partial}{\partial z}\left(b\frac{\partial^2}{\partial r^2} + \frac{1}{r}\frac{\partial}{\partial r} + a\frac{\partial^2}{\partial z^2}\right)\Phi\\
\sigma_z &= \frac{\partial}{\partial z}\left(c\frac{\partial^2}{\partial r^2} + \frac{c}{r}\frac{\partial}{\partial r} + e\frac{\partial^2}{\partial z^2}\right)\Phi\\
\tau_{rz} &= \frac{\partial}{\partial r}\left(\frac{\partial^2}{\partial r^2} + \frac{1}{r}\frac{\partial}{\partial r} + a\frac{\partial^2}{\partial z^2}\right)\Phi
\end{aligned} \tag{5}$$

where

$$\begin{aligned}
a &= (a_{11}a_{13} - a_{12}a_{13})/(a_{11}a_{33} - a_{13}^2)\\
b &= (a_{13}^2 + a_{13}a_{44} - a_{12}a_{33})/(a_{11}a_{33} - a_{13}^2)\\
c &= (a_{11}a_{13} - a_{12}a_{33} + a_{11}a_{44})/(a_{11}a_{33} - a_{13}^2)\\
e &= (a_{11}^2 - a_{12}^2)/(a_{11}a_{33} - a_{13}^2)
\end{aligned} \tag{6}$$

It can be verified that formulating stress components in this way can make the equilibrium equations automatically satisfied [37]. In addition, the compatibility equations can also be satisfied if the arbitrary function Φ is a solution of a modified biharmonic equation:

$$\left(\frac{\partial^2}{\partial r^2} + \frac{\partial}{r\partial r} + \frac{\partial^2}{s_1^2\partial z^2}\right)\left(\frac{\partial^2}{\partial r^2} + \frac{\partial}{r\partial r} + \frac{\partial^2}{s_2^2\partial z^2}\right)\Phi = 0 \tag{7}$$

where

$$s_1^2 = \frac{a+c-\sqrt{(a+c)^2-4e}}{2e} \text{ and } s_2^2 = \frac{a+c+\sqrt{(a+c)^2-4e}}{2e} \tag{8}$$

Note that Lekhnitskii et al. have shown in Ref. [37] that neither s_1 nor s_2 is purely imaginary.

Following the method by which Sneddon solved the isotropic indentation problems [36], we solve this transversely isotropic indentation problem in the Hankel space. Specifically, we take $G(\xi, z)$ as the zero-order Hankel transform, i.e.,

$$G(\xi, z) = \int_0^\infty r\Phi J_0(\xi r)\mathrm{d}r \tag{9}$$

where $J_n(x)$ is the Bessel function of the first kind of order n. Multiplying both sides of Eq. (7) by $rJ_0(\xi r)$ and integrating over the domain of r lead to an ordinary differential equation:

$$\left(\frac{\mathrm{d}^2}{s_1^2\mathrm{d}z^2} - \xi^2\right)\left(\frac{\mathrm{d}^2}{s_2^2\mathrm{d}z^2} - \xi^2\right)G(\xi, z) = 0 \tag{10}$$

Note that this work is limited to the lateral size of the elastic layer that is infinitely large or sufficiently large compared to any horizontal lengths, including the size of the indenter and the Winkler-type length (to be discussed shortly). As long as $s_1 \neq s_2$, integration of Eq. (10) further leads to the solution

$$\begin{aligned} G(\xi, z) = {} & C_1\cosh(s_1\xi z) + C_2\cosh(s_2\xi z) \\ & + C_3\sinh(s_1\xi z) + C_4\sinh(s_2\xi z) \end{aligned} \tag{11}$$

where C_1, C_2, C_3, and C_4 are integration constants to be determined with appropriate boundary conditions. For the problem that we consider in Fig. 1, the four boundary conditions can be specified:

$$\begin{aligned} & [u_z]_{z=d} = 0, \quad [u_r]_{z=d} = 0, \quad [u_r]_{z=0} = 0 \\ & \left[\int_0^\infty r\sigma_z J_0(\xi r)\mathrm{d}r\right]_{z=0} = -\tilde{q} \end{aligned} \tag{12}$$

where the first three equations come from no-slip surfaces on the top and bottom of the layer and the fourth equation is a result of compressive traction $q(r)$ from the deformed plate (note that $\tilde{q}$ is the zero-order Hankel transform of $q(r)$, i.e., $\tilde{q} = \int_0^\infty rqJ_0(\xi r)\mathrm{d}r$). The use of these boundary conditions needs the inverse Hankel transform of the involved components including

$$\begin{aligned} u_r = {} & \frac{(a_{11}-a_{12})(-2a_{13}^2 - a_{44}a_{13} + a_{11}a_{33} + a_{12}a_{33})}{a_{11}a_{33} - a_{13}^2} \\ & \int_0^\infty \xi^2\frac{\mathrm{d}G}{\mathrm{d}z}J_1(\xi r)\mathrm{d}\xi \\ u_z = {} & \int_0^\infty \\ & \xi\left[-\frac{\left(-a_{33}a_{11}^2 + 2a_{11}a_{13}^2 + a_{33}a_{12}^2 - 2a_{12}a_{13}^2\right)}{a_{11}a_{33} - a_{13}^2}\frac{\mathrm{d}^2G}{\mathrm{d}z^2} - a_{44}\xi^2 G\right] \\ & J_0(\xi r)\mathrm{d}\xi \\ \sigma_z = {} & \int_0^\infty \xi\left(\frac{a_{11}^2 - a_{12}^2}{a_{11}a_{33} - a_{13}^2}\frac{\mathrm{d}^3G}{\mathrm{d}z^3} - \frac{a_{13}(a_{11}+a_{12}) + a_{11}a_{44}}{a_{11}a_{33} - a_{13}^2}\xi^2\frac{\mathrm{d}G}{\mathrm{d}z}\right) \\ & J_0(\xi r)\mathrm{d}\xi \end{aligned} \tag{13}$$

Despite the tedious calculations involved in solving the full stress and displacement fields, the mechanical response of the transversely isotropic elastic layer is rather simple, which can be characterized by a spring-like relation in the Hankel space:

$$\tilde{\varsigma}(\xi) = -K(\xi)\tilde{q}(\xi) \tag{14}$$

where $\tilde{\varsigma}$ is the zero-order Hankel transform of $u_z(z = 0, r)$ or $\varsigma(r)$, and K is the Hankel–space Green's function. In particular, we find

$$K(\xi) = \frac{1}{\xi}\frac{1}{(s_1^2 - s_2^2)}\left[\frac{a_{44}(a_{11}a_{33} - a_{13}^2)}{a_{11}^2 - a_{12}^2}\left(\frac{\alpha_1}{s_1\alpha_0} + \frac{\alpha_2}{s_2\alpha_0}\right) + \frac{(2a_{13}^2 - a_{11}a_{33} - a_{12}a_{33})}{(a_{11}+a_{12})}\left(\frac{s_1\alpha_1}{\alpha_0} + \frac{s_2\alpha_2}{\alpha_0}\right)\right] \tag{15}$$

where

$$\begin{aligned} \alpha_0 = {} & \beta_1\sinh(d\xi s_1)\cosh(d\xi s_2) - \beta_2\sinh(d\xi s_2)\cosh(d\xi s_1) \\ \alpha_1 = {} & \beta_1 + \beta_2\sinh(d\xi s_1)\sinh(d\xi s_2) - \beta_1\cosh(d\xi s_1)\cosh(d\xi s_2) \\ \alpha_2 = {} & \beta_2 + \beta_1\sinh(d\xi s_1)\sinh(d\xi s_2) - \beta_2\cosh(d\xi s_1)\cosh(d\xi s_2) \\ \beta_1 = {} & a_{44}(a_{13}^2 - a_{11}a_{33})s_1 - (a_{11}-a_{12})(2a_{13}^2 - a_{11}a_{33} \\ & - a_{12}a_{33})s_1s_2^2 \\ \beta_2 = {} & a_{44}(a_{13}^2 - a_{11}a_{33})s_2 - (a_{11}-a_{12})(2a_{13}^2 - a_{11}a_{33} \\ & - a_{12}a_{33})s_1^2s_2 \end{aligned} \tag{16}$$

We note that in the isotropic case, $s_1 = s_2 = 1$, the solution to Eq. (10) in turn becomes $G_{\mathrm{iso}}(\xi, z) = (D_1 + D_2 z)\cosh(\xi z) + (D_3 + D_4 z)\sinh(\xi z)$. As a consequence, the spring-like elastic response of the layer in Eq. (14) still holds but with

$$K_{\mathrm{iso}}(\xi) = \frac{-(d\xi)^2 + (9 - 24\nu + 16\nu^2)\sinh^2(d\xi)}{2G\xi(1-\nu)[2d\xi + (3-4\nu)\sinh(2d\xi)]} \tag{17}$$

Equation (17) has been reported in [38], which used a slightly different boundary condition (i.e., zero shear stress on the top surface). Its 2D plane-strain or plane-stress version has been discussed in [39]. The result provided in Eq. (15), though appearing too lengthy to be useful, is new to the best of our knowledge.

2.3 Limiting Cases

When the elastic layer is sufficiently thick to be considered as a half-space (i.e., $\xi d \gg 1$), Eq. (15) can be largely simplified to

$$K(\xi d \to \infty) = \frac{G' s_1 s_2 [E'(\nu - 1) + 4G\nu'^2 + 4G\nu\nu'^2] + 2G[2G\nu'^2 - E' + 2G\nu\nu'^2]}{E'^2 G' s_1 s_2 (s_1 + s_2)(\nu - 1)} \frac{1}{|\xi|} \tag{18}$$

which, by setting the material properties isotropic, can be further reduced to

$$K_{\text{iso}}(\xi d \to \infty) = \frac{3 - 4\nu}{4G(1 - \nu)} \frac{1}{|\xi|} \tag{19}$$

This expression can also be obtained by directly taking $\xi d \to \infty$ in Eq. (17). Note that Eq. (19) is different from the classical result $K_{\text{iso}}(\xi d \to \infty) = (1 - \nu)/(G\xi)$ given by Sneddon in [36], which is based on the assumption of no shear stress on the top surface [36], though the two are identical when $\nu = 1/2$[21]. However, our interest in this work is the regime where the elastic layer is rather thin (i.e., $\xi d \ll 1$). In this limit, Eq. (15) becomes ξ-independent at the leading order:

$$K(\xi d \to 0) = \frac{d[E'(\nu - 1) + 4G\nu'^2(\nu + 1)]}{E'^2(\nu - 1)} \tag{20}$$

or simply, after the inverse Hankel transform,

$$q(r) = -\frac{C_{33}}{d} \xi(r) \tag{21}$$

where $C_{33} = E'(1 - \nu)/(1 - \nu - 2E\nu'^2/E')$ is an elastic constant [40]. It is obvious that our approach is not limited to $|\xi d| \ll 1$ as it provides the form shown in Eq. (15) that can be used for elastic layers with arbitrary thickness (even $|\xi d| \gg 1$ as discussed in Eq. (18)). Besides, it is worth noting that using isotropic material properties leads to $K_{\text{iso}}(\xi d \to 0) = (1 - 2\nu)d/[2(1 - \nu)G]$, which has been shown by Skotheim and Mahadevan [19] and extended for nearly incompressible materials by Chandler and Vella [21] and incompressible materials by Dillard [20].

3 Results and Discussion

3.1 The Indentation Problem

Now we return to the indentation problem of a rigid cylindrical indenter on an elastic plate supported by a thin, transversely isotropic elastic layer. We will shortly specify what "thin" means, but for now, let's combine Eqs. (1) for the plate and Eq. (21) for the thin elastic layer to give:

$$B\nabla_{\text{H}}^4 \zeta(r) + k\zeta(r) = -\frac{F\delta_D(r - r_{\text{in}})}{2\pi r_{\text{in}}} \tag{22}$$

where $k = C_{33}/d$, $\delta_D(r)$ is the Dirac delta function, and F is the indentation force required for achieving the prescribed indentation depth δ. We have four natural boundary conditions that can be used to solve Eq. (22):

$$\zeta(r_{\text{in}}) = -\delta, \quad \frac{\mathrm{d}\zeta}{\mathrm{d}r}\Big|_{r=r_{\text{in}}} = 0, \quad \text{and} \quad \zeta, \ \frac{\mathrm{d}\zeta}{\mathrm{d}r} \to 0 \ \text{ as } r \to \infty \tag{23}$$

Equation (22) revokes the classical plate/beam-on-elastic-foundation problem or Winkler's elastic foundation problem [17, 41]. The lateral characteristic length scale, given by the Winkler length, arises immediately as

$$\ell_W = (B/k)^{1/4} = (Bd/C_{33})^{1/4} \tag{24}$$

The use of linear plate theory (with no shear deformation correction) and thin elastic layer approximation can thus be justified by $t, d \ll \ell_W$ [42]. We then rescale the system by introducing the following dimensionless variables:

$$\rho = r/\ell_W, \quad \rho_{\text{in}} = r_{\text{in}}/\ell_W, \quad Z(\rho) = \zeta(r)/\delta, \quad \mathscr{F} = F/(k\ell_W\delta) \tag{25}$$

With these, the problem we consider becomes

$$\frac{\mathrm{d}}{\mathrm{d}\rho}\left\{\rho \frac{\mathrm{d}}{\mathrm{d}\rho}\left[\frac{1}{\rho}\frac{\mathrm{d}}{\mathrm{d}\rho}\left(\rho\frac{\mathrm{d}W}{\mathrm{d}\rho}\right)\right]\right\} + Z = -\frac{\mathscr{F}\delta_D(\rho - \rho_{\text{in}})}{2\pi\rho_{\text{in}}} \tag{26}$$

subject to

$$Z(\rho = \rho_{\text{in}}) = -1, \quad \frac{\mathrm{d}Z}{\mathrm{d}\rho}\Big|_{\rho=\rho_{\text{in}}} = 0, \quad \text{and} \quad Z(\rho \to \infty), \ \frac{\mathrm{d}Z}{\mathrm{d}\rho}\Big|_{\rho\to\infty} \to 0 \tag{27}$$

3.2 Analytical Solutions

The solution to the problem specified in Eqs. (26) and (27) can be readily obtained by realizing that it is also the solution to $\nabla_{\mathrm{H}}^2 Z = \pm \mathrm{i} Z$, where i is the imaginary unit. However, we do not present the full-form solution for various ρ_{in} here; instead, we discuss the solution in two limiting cases: $\rho_{\mathrm{in}} \ll 1$ (the small-indenter-radius limit) and $\rho_{\mathrm{in}} \gg 1$ (the large-indenter-radius limit). Specifically, as $\rho_{\mathrm{in}} \ll 1$, the deflection of the plate is simply

$$Z(\rho) = \frac{2\mathrm{i}}{\pi}\left[K_0\left(\mathrm{e}^{\pi \mathrm{i}/4}\rho\right) - K_0\left(\mathrm{e}^{-\pi \mathrm{i}/4}\rho\right)\right] \tag{28}$$

where K_0 is the second-kind, zero-order modified Bessel function. Its dimensional form reads

$$\zeta(r) = \frac{2\mathrm{i}}{\pi}\left[K_0\left(\mathrm{e}^{\pi \mathrm{i}/4} r \Big/ \ell_W\right) - K_0\left(\mathrm{e}^{-\pi \mathrm{i}/4} r \Big/ \ell_W\right)\right]\delta \tag{29}$$

The required indentation force can be calculated by either using the condition of local shear force balance at $r = r_{\mathrm{in}}$ or equivalently summing up the restored forces due to the deformation of the spring-like elastic layer, i.e.,

$$F = -2\pi \int_0^\infty k\zeta(r) r \mathrm{d}r = 8B\delta \Big/ \ell_W^2 \tag{30}$$

which suggests a linear relationship between indentation force and depth with the coefficient being contributed by the elasticity of both the plate and the thin layer. We then define the indentation stiffness as

$$\kappa_s(\rho_{\mathrm{in}} \to 0) = \frac{F}{\delta} = 8\left(\frac{BC_{33}}{d}\right)^{1/2} \tag{31}$$

In the opposite limiting case where $r_{\mathrm{in}} \to \infty$, the bending effect of the plate should be negligible. We then obtain the indentation force by simply summing the pressure that compresses the elastic layer with a uniform deformation of δ in the region $r < r_{\mathrm{in}}$. Specifically, we have $F = \pi r_{\mathrm{in}}^2 \cdot k\delta = \pi C_{33} r_{\mathrm{in}}^2 \delta \Big/ d$ and the indentation stiffness

$$\kappa_s(\rho_{\mathrm{in}} \to \infty) = \pi C_{33} r_{\mathrm{in}}^2 \Big/ d \tag{32}$$

These results conclude the analytical progress made in this work. In particular, the simplicity of the approximate theory for the thin, transversely isotropic elastic layer in Eq. (14) allows analytical solutions for indenters of any axisymmetric shape and size. However, in this subsection, we focus solely on the small- and large-indenter limits for demonstration purposes.

3.3 Comparison with Numerical Results

We then utilize the finite element method to validate our approximate theory for the indentation response of a plate on a transversely isotropic elastic layer. Following the model problem discussed in the previous section, we fix the displacement of the bottom surface of the elastic layer and apply a uniform displacement in the region $r < r_{\mathrm{in}}$ on the top surface of the elastic plate to simulate the action of a frictionless, rigid cylindrical indenter. The plate and layer are perfectly bonded. Refined meshes around $r = r_{\mathrm{in}}$ are used to ensure the convergence of the computed results. Three sets of material properties are employed, as detailed in Table 1. Specifically, the material properties of the elastic plate and the elastic layer in Case 1 are similar to those of Cu and PDMS, respectively. Cases 2 and 3 approximate Au on Ecoflex, with variations in the thicknesses of the plates and elastic layers. Note that all elastic layers in these cases are deliberately set to be transversely isotropic.

The indentation force–displacement relationship and the deflection of the elastic plate are among the most experimentally accessible data. In Fig. 2, we present both the dimensional and dimensionless indentation force–displacement relationships, along with the shape of the deformed plate when the applied load is a point force (i.e., $r_{\mathrm{in}} \to 0$). The markers denote finite element analysis (FEA) results obtained using material parameters summarized in Table 1. The solid lines are all based on analytical expressions in Eqs. (29) and (30).

Excellent agreement is found between analytical results based on linear plate theory and approximate thin elastic layer and numerical results. In particular, as suggested by Eq. (30), rescaling the force and indentation depth as $F \Big/ (BC_{33} d)^{1/2}$ and $\delta \Big/ d$ in Fig. 2c, respectively, can collapse the data obtained from materials of different geometric and mechanical properties in Fig. 2a onto a single master curve. Similarly, the deformed shape of the plate in various cases can collapse by using ℓ_W as the characteristic length (see Fig. 2d).

We then move on to investigate the effect of the size of the indenter on the indentation stiffness defined by $F \Big/ \delta$ in Fig. 3. In particular, we rewrite the dimensionless indentation stiffness at the small and large indenter limits as

$$\hat{\kappa}_s = \frac{\kappa_s}{(BC_{33} \Big/ d)^{1/2}} = \begin{cases} 8, & r_{\mathrm{in}} \Big/ \ell_W \ll 1 \\ \pi (r_{\mathrm{in}} \Big/ \ell_W)^2, & r_{\mathrm{in}} \Big/ \ell_W \gg 1 \end{cases} \tag{33}$$

Figure 3 presents the solutions (denoted by dashed and dotted curves) at two limits as well as FEA results (denoted by markers) calculated based on material properties specified in Table 1. We find good agreement between Eq. (33) and numerical results at the small and large indenter limits.

Table 1 A summary of geometric and mechanical parameters of the plate on a transversely isotropic elastic layer in our finite element calculations

	t (μm)	E_c (GPa)	ν	d (μm)	C_{11} (MPa)	C_{12} (MPa)	C_{13} (MPa)	C_{33} (MPa)	C_{44} (MPa)
Case 1	5	124	0.3	15	8.8617	3.0924	1.315	2.7893	1.1261
Case 2	5	79	0.3	15	0.0683	0.0221	0.01	0.0422	0.018
Case 3	10	79	0.3	20	0.0683	0.0221	0.01	0.0422	0.018

The plate is linear, elastic, and isotropic, so its bending rigidity is $B = E_c t^3 \big/ [12(1-\nu^2)]$, where E_c, t, and ν are the elastic modulus, thickness, and Poisson's ratio of the plate, respectively. C_{ij} are the elastic constants for the elastic layer

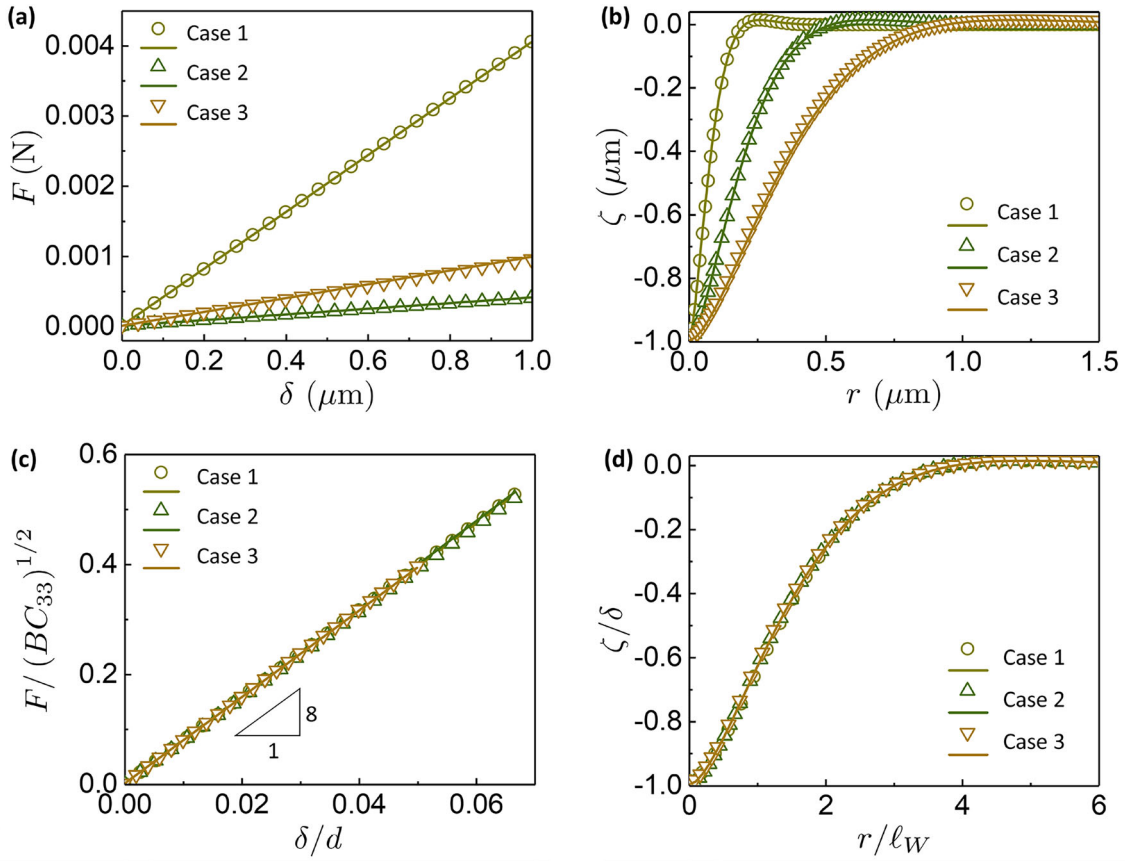

Fig. 2 Mechanical response of plate on transversely isotropic elastic layers under point loads: **a** dimensional indentation force as a function of indentation depth for three sets of material parameters summarized in Table 1; **b** dimensional deflection of the plate when $\delta = 1\,\mu$m; **c** dimensionless indentation force $F\big/(BC_{33}d)^{1/2}$ as a function of dimensionless indentation depth $\delta\big/d$; **d** normalized plate deflection $\zeta\big/d$ as a function of rescaled radial position $r\big/\ell_W$. Here we only show the data obtained under $\delta = 1\,\mu$m. Solid curves in (**a**, **c**) and (**b**, **d**) are from Eqs. (30) and (29), respectively. The empty markers denote FEA results

Interestingly, a nonlinear combination of the solutions at the two limits

$$\hat{\kappa}_s = \left[8^{3/5} + (\pi^2 r_{\text{in}}\big/\ell_W)^{3/5}\right]^{5/3} \tag{34}$$

provides a good approximation for the indentation stiffness for any size of indenter radius (the error is found within 10%).

3.4 Breakdown of Approximate Solutions

Finally, we discuss the validity of our approximate solutions to the indentation problem. First of all, the thickness of the plate should be small relative to ℓ_W, which could often be satisfied in experiments such as piezoresistive tests [6]. Besides, the derivation of the simplified form in Eq. (21) has relied on the assumption of $\xi d \ll 1$. This assumption is reasonable only when $d \ll \max\{r_{\text{in}}, \ell_W\}$, i.e.,

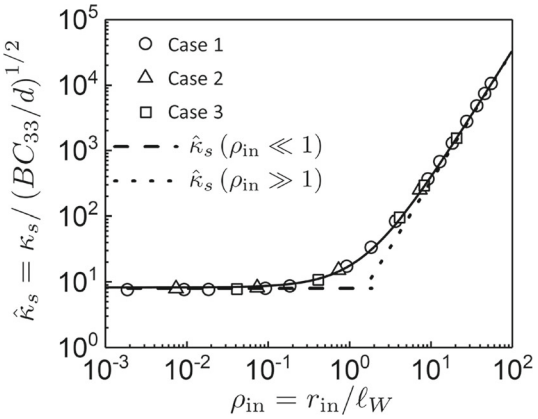

Fig. 3 The dimensionless indentation stiffness $\hat{\kappa}_s = \kappa_s / (BC_{33}/d)^{1/2}$ as a function of the radius of the indenter, r_{in}/ℓ_W. Markers denote FEA results based on material properties summarized Table 1. The dashed and dotted curves are based on Eq. (33), while the solid curve is a nonlinear combination of the two solutions given by Eq. (34)

$$d \ll \max\left\{r_{\text{in}},\ (Bd/C_{33})^{1/4}\right\} \tag{35}$$

Therefore, the thin elastic layer approximation can be achieved when the elastic layer is physically thin, the indenter radius is large, the stiffness of the elastic layer is small, or the bending rigidity of the plate is large.

To illustrate this criterion, we use the material parameters specified in Case 1 of Table 1 and vary the thickness of the elastic layer for FEA calculations, as shown in Fig. 4a. Two indenter sizes are used: $\rho_{\text{in}} = 0$ (denoted by circles) and $\rho_{\text{in}} = 5d/\ell_W$ (denoted by squares). It can be found that in the case of $\rho_{\text{in}} = 0$, the analytical solution at the small indenter limit given in Eq. (33) breaks down as d/ℓ_W is around the unit. By contrast, the solution for $\rho_{\text{in}} \gg 1$ remains accurate for square markers even when the elastic layer is no longer thin relative to ℓ_W. This is because the criterion in Eq. (35) is approximately satisfied by $d \ll r_{\text{in}}$.

An alternative way to tune d/ℓ_W is by fixing d and varying the elastic modulus of the plate E_c, which in turn, affects its bending rigidity $B = E_c t^3/[12(1-\nu^2)]$, where t and ν are the thickness and Poisson's ratio of the plate, respectively. The FEA result in Fig. 4b is calculated this way under a point load (i.e., $\rho_{\text{in}} = 0$). In this case, the deviation between the analytical solution ($\hat{\kappa}_s = 8$) and numerical results occurs at lower values of d/ℓ_W compared to Fig. 4a. Additionally, the deviation in Fig. 4a is due to the analytical solution overestimating the indentation stiffness, in contrast to the underestimation observed in Fig. 4a. This suggests that the deformation of the plate itself becomes significant at small E_c [43], a factor not accounted for in the model.

4 Conclusion

In this study, we have investigated the indentation response of an elastic plate resting on a thin, transversely isotropic elastic layer supported by a rigid substrate using transform methods. Our results have included developing the linear normal force–deformation relation for a transversely isotropic elastic layer of finite thickness in the Hankel space and then applying this relation to understand the indentation force-depth

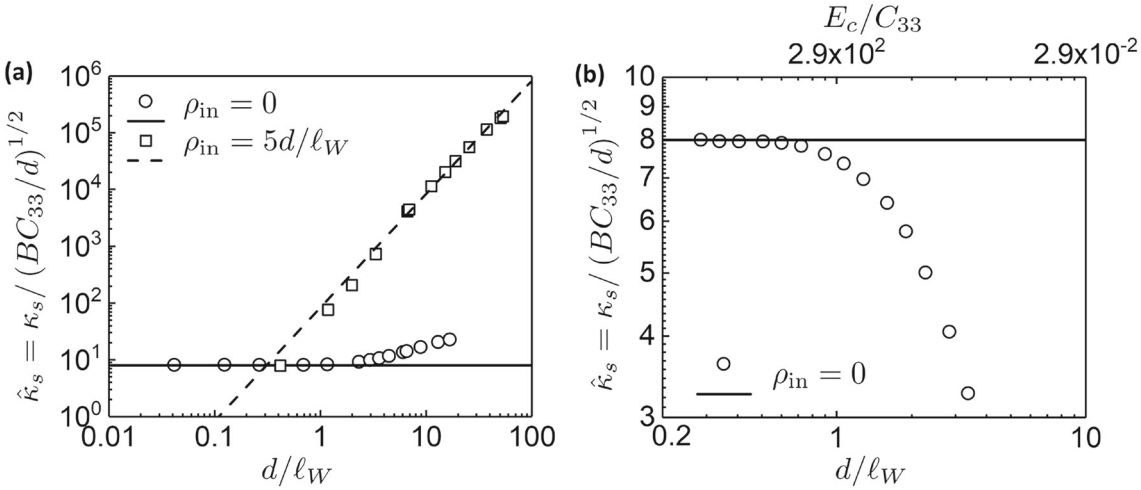

Fig. 4 The effect of the thickness of the elastic layer on the indentation stiffness: **a** dimensionless indentation stiffness as a function of rescaled elastic layer thickness d/ℓ_W for a point load (circles) and indenter radius of $r_{\text{in}} = 5d$ (squares). Markers are FEA results calculated based on material parameters in Case 1 of Table 1 (except that varying d is used). The solid and dashed curves are given by the small and large indenter limits in Eq. (33), respectively. **b** Dimensionless indentation stiffness as a function of rescaled elastic layer thickness d/ℓ_W for a point load. The material parameters are given in Case 1 of Table 1 except that we vary the elastic modulus of the plate E_c to modify ℓ_W and thus d/ℓ_W

relation for plates on transversely isotropic elastic layers. The analytical solutions in large and small indenter limits have been provided and also validated against numerical calculations using finite element methods. We have found good agreement between analytical predictions and numerical calculations as long as the system maintains sufficiently slender and the plate is sufficiently stiff. These results offer significant quantitative insights into the mechanical behavior of many transversely isotropic semiconductor materials, which are commonly employed in slender geometries and coated with an elastic conductive layer in applications such as electronic devices.

Acknowledgements This research was financially supported by the National Natural Science Foundation of China (12372103), the Opening Fund of State Key Laboratory of Nonlinear Mechanics (Institute of Mechanics, CAS), and the Fundamental Research Funds for Central Universities (Peking University).

Declarations

Conflict of interest The authors declare that they have no known competing financial interests or personal relationships that could have appeared to influence the work reported in this paper.

References

1. Dai Z, Liu L, Zhang Z. Strain engineering of 2d materials: issues and opportunities at the interface. Adv Mater. 2019;31:1805417.
2. Akinwande D, Brennan CJ, Bunch JS, Egberts P, Felts JR, Gao H, Huang R, Kim JS, Li T, Li Y, et al. A review on mechanics and mechanical properties of 2d materials—graphene and beyond. Extreme Mech Lett. 2017;13:42–77.
3. Liu M, Li X. Mechanical properties measurement of materials and devices at micro-and nano-scale by optical methods: a review. Opt Lasers Eng. 2022;150: 106853.
4. Liu L, Liu H, He Y, Liu D. Mechanics and topology of twisted hyperelastic filaments under prescribed elongations: Experiment, theory, and simulation. J Mech Phys Solids. 2024;182: 105478.
5. Peng G, Liu Y, Xu F, Jiang H, Jiang W, Zhang T. On determination of elastic modulus and indentation hardness by instrumented spherical indentation: influence of surface roughness and correction method. Mater Res Express. 2023;10: 086503.
6. Wang B, Li J, Fang Z, Jiang Y, Li S, Zhan F, Dai Z, Chen Q, Wei X. Large and pressure-dependent c-axis piezoresistivity of highly oriented pyrolytic graphite near zero pressure. Nano Lett. 2024;24:4965–71.
7. Chen E, Dai Z. Axisymmetric peeling of thin elastic films: A perturbation solution. J Appl Mech. 2023. https://doi.org/10.1115/1.4062831.
8. Yang L, Yue S, Tao Y, Qiao S, Li H, Dai Z, Song B, Chen Y, Du J, Li D, et al. Suppressed thermal transport in silicon nanoribbons by inhomogeneous strain. Nature. 2024;629:1–6.
9. Mansfield EH. The bending and stretching of plates. Cambridge: Cambridge University Press; 1989.
10. Androulidakis C, Zhang K, Robertson M, Tawfick S. Tailoring the mechanical properties of 2d materials and heterostructures. 2D Mater. 2018;5:032005.
11. Dai Z, Lu N. Poking and bulging of suspended thin sheets: Slippage, instabilities, and metrology. J Mech Phys Solids. 2021;149: 104320.
12. Wang G, Dai Z, Xiao J, Feng S, Weng C, Liu L, Xu Z, Huang R, Zhang Z. Bending of multilayer van der waals materials. Phys Rev Lett. 2019;123: 116101.
13. Han E, Yu J, Annevelink E, Son J, Kang DA, Watanabe K, Taniguchi T, Ertekin E, Huang PY, van der Zande AM. Ultrasoft slip-mediated bending in few-layer graphene. Nat Mater. 2020;19:305–9.
14. Gao Y, Kim S, Zhou S, Chiu HC, Nélias D, Berger C, De Heer W, Polloni L, Sordan R, Bongiorno A, et al. Elastic coupling between layers in two-dimensional materials. Nat Mater. 2015;14:714–20.
15. Akinwande D, Petrone N, Hone J. Two-dimensional flexible nanoelectronics. Nat Commun. 2014;5:5678.
16. Dai Z, Lu N, Liechti KM, Huang R. Mechanics at the interfaces of 2D materials: Challenges and opportunities. Curr Opin Solid State Mater Sci. 2020;24: 100837.
17. Dillard DA, Mukherjee B, Karnal P, Batra RC, Frechette J. A review of Winkler's foundation and its profound influence on adhesion and soft matter applications. Soft Matter. 2018;14:3669–83.
18. Boussinesq J. Equilibre d'elasticite d'un solide isotrope sans pesanteur, supportant differents poids, C. Rendus Acad. Sci. 1878.
19. Skotheim J. Mahadevan L Soft lubrication. Phys Rev Lett. 2004;92: 245509.
20. Dillard D. Bending of plates on thin elastomeric foundations. J Appl Mech. 1989;56:382–6.
21. Chandler TG, Vella D. Validity of Winkler's mattress model for thin elastomeric layers: beyond Poisson's ratio. Proceedings of the Royal Society A. 2020;476:20200551.
22. Movchan AB, Rebrov KR, Rodin GJ. Axisymmetric deformation of compressible, nearly incompressible, and incompressible thin layers between two rigid surfaces. Int J Solids Struct. 2021;214:61–73.
23. Movchan A, Movchan N, Rodin G. Asymptotic analysis of thin linear elastic layers constrained by two rigid plates. Int J Solids Struct. 2023;285: 112561.
24. Ding H, Chen W, Zhang L. Elasticity of transversely isotropic materials. New York: Springer Science & Business Media; 2006.
25. Mandriota N, Friedsam C, Jones-Molina JA, Tatem KV, Ingber DE, Sahin O. Cellular nanoscale stiffness patterns governed by intracellular forces. Nat Mater. 2019;18:1071–7.
26. Gudmundsson GH, Paolo FS, Adusumilli S, Fricker HA. Instantaneous antarctic ice sheet mass loss driven by thinning ice shelves. Geophys Res Lett. 2019;46:13903–9.
27. Elliott AH. Axial symmetric stress distributions in aeolotropic hexagonal crystals. The problem of the plane and related problems. Math Proc Cambridge Philos Soc. 1949;45:621–30.
28. Fabrikant IV. Elastic field around a circular punch. J Appl Mech. 1988;55:604.
29. Hanson MT. The elastic field for spherical hertzian contact including sliding friction for transverse isotropy. J Tribol. 1992;114:606–11.
30. Hanson TM. The elastic field for conical indentation including sliding friction for transverse isotropy. J Appl Mech. 1992;59:S123–30.
31. Ding H, Xu B. General solutions of axisymmetric problems in transversely isotropic body. Appl Math Mech. 1988;9:143–51.
32. Yu H, Sanday S, Rath B, Chang C. Elastic fields due to defects in transversely isotropic bimaterials. Proc R Soc Lond Ser A: Math Phys Sci. 1995;449:1–30.
33. Yu H. A concise treatment of indentation problems in transversely isotropic half-spaces. Int J Solids Struct. 2001;38:2213–32.
34. Ning X, Lovell M, Slaughter WS. Asymptotic solutions for axisymmetric contact of a thin transversely isotropic elastic layer. Wear. 2006;260:693–8.
35. Argatov I, Mishuris G, Argatov I, Mishuris G. Deformation of a thin bonded transversely isotropic elastic layer. In: Contact mechanics of articular cartilage layers: asymptotic models. Cham: Springer; 2015. p. 1–18.

36. Sneddon IN. Fourier Transforms. Courier Corporation. 1995.
37. Lekhnitskii SG, Fern P, Brandstatter JJ, Dill E. Theory of elasticity of an anisotropic elastic body. Phys Today. 1964. https://doi.org/10.1063/1.3051394.
38. Ai Z, Yue Z, Tham L, Yang M. Extended Sneddon and Muki solutions for multilayered elastic materials. Int J Eng Sci. 2002;40:1453–83.
39. Hannah M. Contact stress and deformation in a thin elastic layer. Q J Mech Appl Math. 1951;4:94–105.
40. Argatov I, Mishuris G. Axisymmetric frictionless indentation of a transversely isotropic elastic half-space. Springer: Springer International Publishing; 2018.
41. Wang Y, Tham L, Cheung Y. Beams and plates on elastic foundations: a review. Prog Struct Mat Eng. 2005;7:174–82.
42. Audoly B, Pomeau Y. Elasticity and geometry. In: Peyresq lectures on nonlinear phenomena. New Jersey: World Scientific; 2000. p. 1–35.
43. Box F, Jacquemot C, Adda-Bedia M, Vella D. Cloaking by coating: how effectively does a thin, stiff coating hide a soft substrate? Soft Matter. 2020;16:4574–83.